Development of a Real-time Point Tracker System for MAV Wind Tunnel Tests using Commercial Video Cameras

Hong-Il Kim[1], Ho-Young Kim[1], Hyun-Jin Park[1], Jun-Bum Kim[2], Do-Hyung Kim[3], Jeongho Han[4], and Jae-Hung Han[1†]

[1] Div. of Aerospace Engineering, KAIST, Daejeon, Korea
(Tel : +82-42-350-3723; E-mail: jaehunghan@kaist.ac.kr)
[2] Div. of Mechanical Engineering, KAIST, Daejeon, Korea
[3]Korea Aerospace Research Institute, Daejeon, Korea
[4]Agency for Defense Development, Daejeon, Korea

Abstract: The purpose of this research is to develop a real-time point tracker system for wind tunnel testing using commercial video cameras. Recently, many kinds of MAVs (Micro aerial vehicles) are developed using fixed, flapping and rotating wings. However, unlike typical airplanes, MAV wings are more flexible and there will be continuous deformations along the wings depending on flight conditions. Therefore, it is interesting to measure the real-time deformation of the wings during a wind-tunnel test. Typical surface deformation measurement systems based on optical image processing techniques have been widely used in wind tunnel tests; a SPR (Stereo Pattern Recognition) system and PMI (Projection Moiré Interferometry) system have been used to measure the structural deformation of aerodynamic surfaces such as wings and blades. These systems, however, are very costly to perform the wind-tunnel tests of the small scale MAVs because complex optical components such as large flashes, high-resolution cameras and data acquisition systems with several computers are required. We developed a real-time point tracker system using commercial cameras. This system used IR LEDs and commercial IR CCD cameras to minimize interferences posed by other light sources. The main algorithm used for this system is an optical point tracking algorithm, which is composed of the point extraction algorithm and the points matching algorithm for 3-D motion estimation. A series of verification tests have been performed. Then, the developed real-time point tracker system was applied to measure deformations of the tail wing of the Smart Flapper developed in KAIST while MFC (Micro-Fiber Composite) actuators are controlling the curvature of the tail-wing in the low-speed wind tunnel.

Keywords: 3-D position estimation algorithm, Specific point extraction algorithm, MAV (Micro aerial vehicle), Wind-tunnel test, Flexible wing deformation, MFC (Micro-Fiber Composite) actuator

1. INTRODUCTION

Micro air vehicles (MAVs) have been investigated by many researchers since the mid-1990s. In the beginning, many MAVs developed had a fixed wing-body configuration. This fixed wing-body configuration originated from conventional wing-body aircraft, and was used for increasing lift while ensuring sufficient payload space for electronics. However, the fixed wing-body configuration loses its efficiency in low Reynolds number regime. MAVs are nominally 150mm in their largest dimension and fly at or below speeds of ~40 km/h, resulting in lower Reynolds number conditions. Therefore, many researchers have investigated new types of MAVs with inspirations from birds, insects and bats, whose flight regime is similar to MAVs', for enhancing the flight capabilities. One of the unique features of bio-inspired MAVs is that they have highly flexible wings with large motions such as flapping, twisting and so on. The flexibility of the wing allows the MAVs to utilize the delayed stall at the high angle of attack (AoA) maneuver while the wings are being deformed. In addition, the flexibility leads more stable, controllable flight against to abrupt wind gusts. However, the deformable wing geometry makes the difficulties for understanding the aerodynamic characteristics and flight dynamics. Therefore, it is very helpful to understand the roles of wing flexibility on enhanced aerodynamics and stability if we can acquire the deformed shapes of the wing in flight conditions.

Typical shape measurement techniques such as PGM (Projected Grid Mehod), PMI (Projection Moiré Interferometry) and SPR (Stereo Pattern Recognition) have been used in several wind tunnel tests. Van der Draai *et al* [1] described two different Moiré techniques such as Painted Pattern Method (PaPM) and Projection Pattern Method (PrPM) for the deformation measurements of a dummy wing. Fleming *et al* [2-3] used the PMI to obtain near instantaneous blade deformations for HART-I (Higher harmonic control Aero-acoustic Rotor Test). PMI was also applied to measure the structural deformation of MAV wings during a series of wind tunnel tests as shown in Fig.1. However, it is very difficult to apply such projection methods for the MAVs whose wing motions include the rigid body motions such as flapping and lead-lag motion and so on. SPR (Stereo Pattern Recognition) method was also introduced to measure the wing motions. Schneider [4] applied SPR method, where 3-D positions of several markers were traced, to rotating blades for HART-II project.

(a) (b)

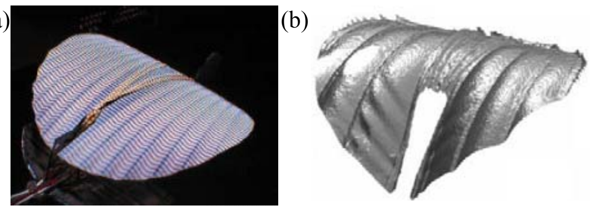

Fig. 1 (a) MAV with PMI projection grid lines [3]
(b) 3-D representation of MAV wind shapes measured by PMI [3]

These systems, however, require complex optical components such as large flashes, high-resolution cameras and data acquisition systems with several computers. These systems are very costly to perform the wind-tunnel tests of the small scale MAVs. Thus, in this study, a real-time point tracker system using commercial cameras was developed using commercial four CCDs and IR LEDs. The software was composed of a specific point extraction algorithm and a specific point matching algorithm, which allowed the calculation of 3-D coordinates. After configuring the point tracker system, a series of verification tests have been performed to evaluate the system performance. Then, the developed real-time point tracker system was applied to measure deformations in the tail wing of the Smart Flapper which was developed in KAIST while MFC (Micro-Fiber Composite) actuators are controlling the curvature of the tail-wing in the low-speed wind tunnel.

2. THE PRINCIPLE OF 3-D POINT TRACKING

By using multiple cameras, 3-D coordinates of the points are precisely obtained using a specific point extraction algorithm and a 3-D position estimation algorithm in sequence with camera calibration data as in Fig. 2.

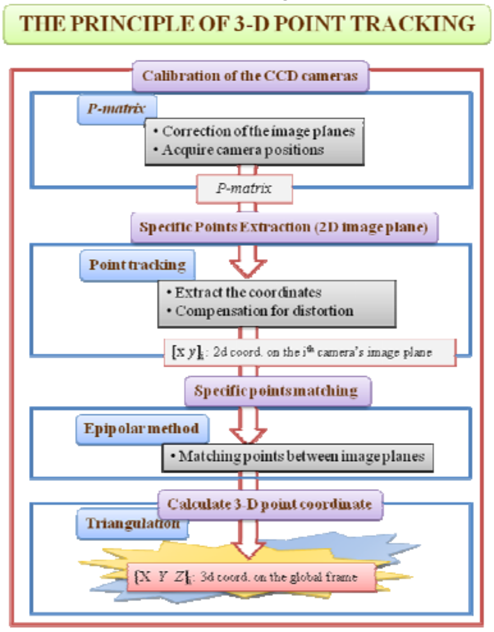

Fig. 2 The calculation process of 3-D point tracking

2.1 Calibration of the CCD cameras

The camera is the apparatus which maps the 3-D real world $(X,Y,Z)^T$ into a 2-D image $(x,y)^T$ as expressed in eq. (1). The mapping characteristics of each camera are contained in camera projection matrices (*P-matrices*). In case of general camera projection matrix *P-matrices* is composed of camera calibration matrix $K_{3\times 3}$ which implies the intrinsic parameters of the camera and rotation matrix $R_{3\times 3}$ and translation matrix $T_{3\times 1}$ which stand for extrinsic parameters between cameras as eq. (2). For a real CCD camera, *P-matrix* is expressed using new camera calibration matrix K as shown in eq. (3).

$$(X,Y,Z)^T \Rightarrow (x,y)^T \qquad (1)$$

$$P = K[R \mid t] \qquad (2)$$

$$\hat{x} = \begin{bmatrix} \alpha_x & s & x_0 \\ & \alpha_y & y_0 \\ & & 1 \end{bmatrix} [R \mid t] \begin{pmatrix} X \\ Y \\ Z \\ 1 \end{pmatrix} \qquad (3)$$

where α_x, α_y are the focal lengths in pixel dimensions, m_x, m_y are the number of pixels per unit distance along x and y direction, x_0, y_0 are the position of the principal points in pixel dimensions and s is the skew parameter. This *P-matrix* including K, R and t matrices of the CCD used in this study, were obtained using *Camera Calibration Toolbox* in MATLAB [5].

2.2 Specific Points Extraction

In this step, 2-D coordinates of the specific points are obtained in pixel dimensions of each camera. We used IR illuminations and attached reflective markers on the structure surfaces to easily distinguish the markers because the markers appear much brighter than the rest parts of the image. The exact positions of the markers, the center positions of the brighter spots, are calculated using the Gaussian mask method as explained in Fig. 3.

Fig. 3 Specific point (Marker reflection) extraction

2.3 Specific points matching using epipolar geometry

Before calculating the 3-D coordinates of specific points, the 2-D coordinates of random points in image planes of cameras should be matched each other. Usually, the epipolar constraint is used to perform the specific points matching. Because the epipolar constraint implies that the point of interest and the projected points of multiple cameras should lie on the same plane (epipolar plane in Fig. 4), we can obtain matched specific points in 2-D coordinate of image planes from the epipolar constraint. The epipolar constraint is expressed in eq. (4) using camera rotation matrix R and translation matrix t.

$$P_1^T R[t]_X P_2 = 0 \qquad (4)$$

where P_1 and P_2 represent the specific points on the image planes and $[]_x$ represents the cross product.

2.4 Calculation of 3-D coordinates of matched points

Generally, the concept of triangulation is applied to calculate the 3-D coordinates of the matched points. Theoretically, the back-project rays should meet at one point (*G* point in Fig. 4), but the errors always exist. Thus, the point whose 3-D position is closest to back-project rays of specific points in image planes is obtained as depicted in Fig. 5. The optimum point is searched by minimizing the total distance *D*.

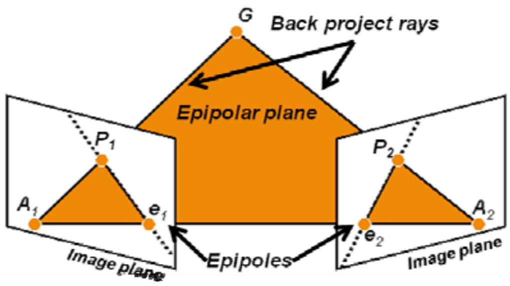

Fig. 4 Epipolar geometry [6]

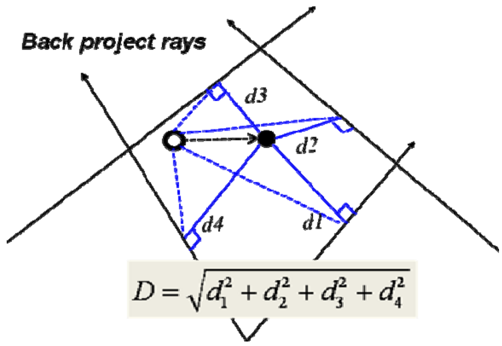

Fig. 5 Calculation of 3-D coordinates of specific points

3. SYSTEM PREPARATION

We prepared a real-time point tracker system using four-CCD cameras with single personal computer for enhancing the point track accuracy. IR LEDs were attached to the CCD cameras for illumination, and CCD cameras were modified to detect only IR light, because it is more comfortable and easier to detect IR light than visible light in room condition.

3.1 System configuration

Microsoft's VX-3000 webcam, one of the commercially available cameras, was used for CCD camera systems in this study. The VX-3000 uses USB 1.1 technology and has a resolution of 640*480 pixels. Its highest frame rate is 30 frames per second. In order to make it easier to find points of interest and to decrease the influence of exterior light, infrared lights and reflective paper were used. Originally, VX-3000 webcam is unable to detect infrared light because they have IR filters to prevent color distortions when displaying images within the visible light spectrum. So, the infrared filters were removed and were replaced with filters that block visible light. The reflective paper was stuck onto points that were to be tracked, and IR LEDs were attached to the front of the cameras. The diodes were SI3317-H diodes manufactured by AUX and have a range of 850mm. Fig. 5 shows the prepared cameras and IR illumination composed of IR LEDs and Fig. 6 shows the reflective markers on the interesting points of the wing.

3.2 Software development

As mentioned before, the software used in cameras is composed of two parts: the first part computes 2-D dimensional pixel data and the second part calculates the 3-D coordinates. The program uses a 'Specific point extraction algorithm' to extract the points reflected from the markers to subsequently find the 2-D pixel coordinates of the points of interest on the image plane and to correct for spherical aberrations. The 2-D pixel coordinates, if within an error range, are grouped with coordinate values that were recorded in a similar timeframe then analyzed through a 'Specific point matching algorithm' and 'Triangulation'. The final results are the 3-D coordinates of the points. Fig. 7 is the screenshot of the developed software.

3.3 System verification test

A series of verification tests have been performed in order to evaluate the uncertainties of the system. For a 3-D point tracking, both orthogonal direction and parallel direction to the image plane should be measured successfully as depicted in Fig. 8. Thus, in this verification test, we prepared the vernier calipers and micrometers for making parallel motion and orthogonal motion of reflective marker, respectively. The vernier calipers and micrometer were set on a stationary clamp so that one end could slide out. Small sections of reflective paper were affixed to the movable ends. The caliper and micrometer were placed in front of the camera system, so the reflective paper could be moved by exact measures. Fig. 10 shows the measured displacement when the end of the caliper traveled 1mm, 10mm and 20mm along the orthogonal direction. Fig. 11 shows the histograms of the measured displacement of the caliper which traveled 1mm, 10mm and 20mm along the parallel direction. From the results, the parallel and orthogonal travels of the reflective marker were successfully estimated using developed point tracker system.

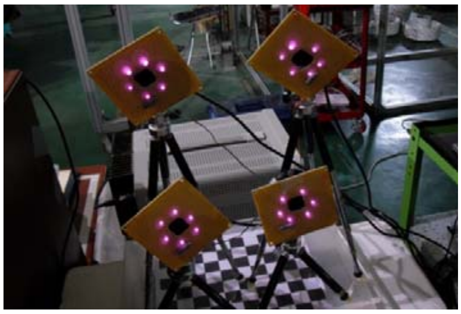

Fig. 5 VX-3000 webcams with IR LEDs

Fig. 6 Attached reflective markers on the wing surface

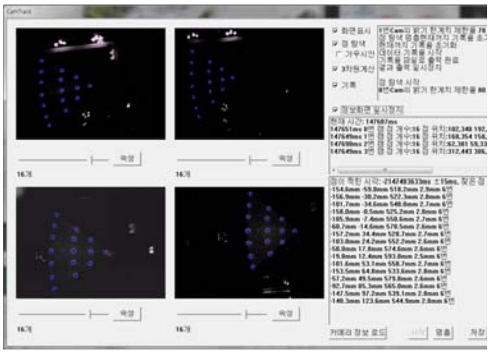

Fig. 7 Screenshot of the developed software

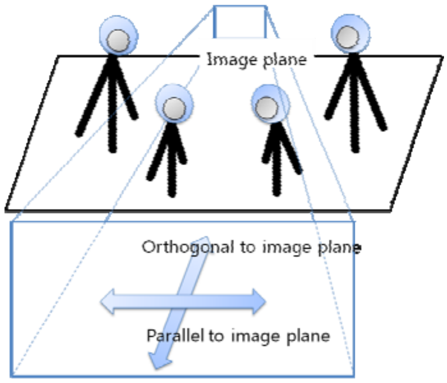

Fig. 8 Verification for orthogonal and parallel directions

Fig. 9 The vernier calipers with reflective paper attached for parallel direction test

For a quantitative aspect, the errors and standard deviations were presented in Table 1. From the table, the maximum error is 0.34mm and maximum standard deviation is 0.36mm. These results imply that developed point tracker system might insure the measurement uncertainty under 0.5mm. Comparing to the SPR system, whose resolution is 0.4mm, used in HART-II program, it is remarkable performance. Therefore, the developed point tracker system could be used for small MAVs test.

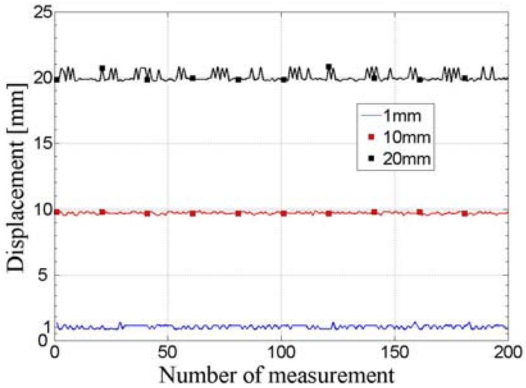

Fig. 10 Measurement results for orthogonal travels of the reflective marker

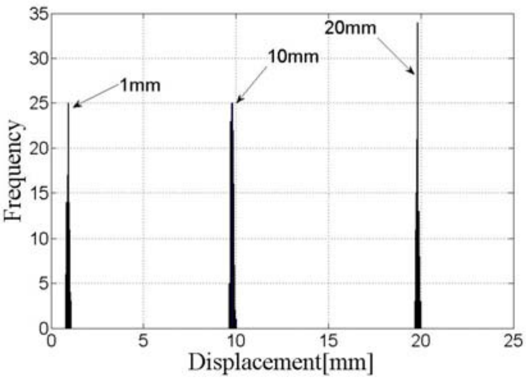

Fig. 11 Histograms for parallel travels of the reflective marker

Table 1 Measurement results: errors & standard deviations

	Travel [mm]	Errors[mm]	STD [mm]
Parallel direction	1.00	-0.07	0.13
	10.00	-0.21	0.16
	20.00	-0.18	0.13
Orthogonal direction	1.00	0.12	0.18
	10.00	-0.34	0.12
	20.00	-0.18	0.36
Measurement uncertainty		0.50mm $\approx \sqrt{0.34^2 + 0.36^2}$	

4. EXPERIEMENTS

The deformations of the Smart Flapper's tail wing were measured using the developed real-time point tracker system in a low-speed wind tunnel section with varying the wind speeds and MFC (Micro-Fiber Composite) actuations.

4.1 Experimental setup

The experiments were performed in the low-speed wind tunnel which has an open type test section with 300mm ×300mm×1000mm dimensions, the flow speed range from 1 to 30m/s and turbulent intensity of less than 0.5% at 30m/s) in KAIST. The camera system composed of four cameras arranged in a rectangular formation as shown in Fig. 5. The camera system is placed on a separate acryl plank, which is placed next to the wind tunnel. The tail-wing (explained in section 4.2) is placed inside the wind tunnel vertically as in Fig. 12. The cameras are oriented towards the wing, which lies approximately 30-40 cm from where the cameras are placed. The total experimental setup including power amplifier for MFC actuator is depicted in Fig. 13.

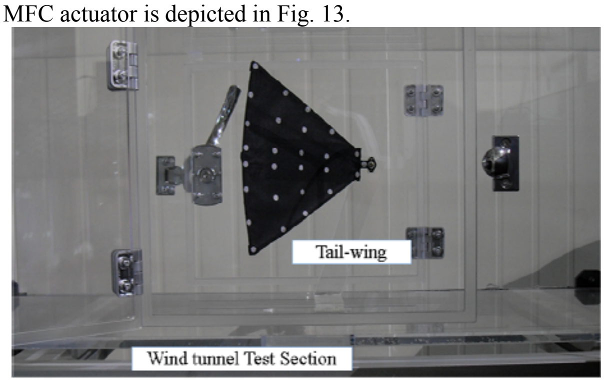

Fig. 12 Fixed tail wing with reflective markers in wind tunnel

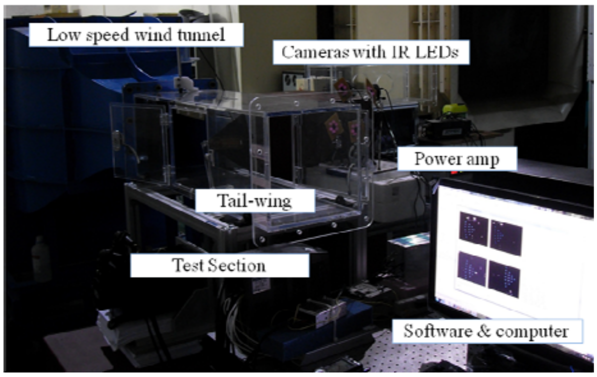

Fig. 13 Total experimental setup

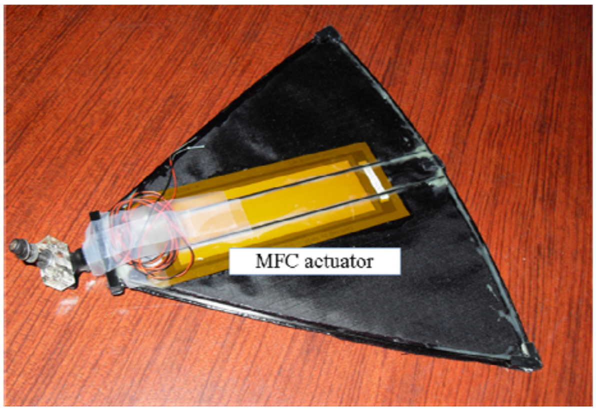

Fig. 14 Tail wing bottom side with MFC actuator

4.2 Experiments

The tail wing consists of composite frames, flexible Nylon-ribstop skin and MFC (M8557P1) actuator (Fig. 14). The wing was then attached to an apparatus that allows it to maintain a vertical position so the cameras can see the 16 markers affixed to the wing surface (Fig. 15). The experiments were executed for measuring tail wing deformed shapes as varying wind speed and input voltage of MFC actuator. Test conditions are listed in Table 2. At 'pure wind' condition, wing deformation was measured to find the deformed shapes according to the wind speeds; similarly, the 'pure actuation' condition was also dealt with to find the induced deformation of the wing by MFC actuator. The 'wind+actuation' condition was also treated to understand how much deformation can be induced by MFC actuator under the free stream.

Table 2 Test conditions

Test conditions	Wind speeds	Input voltage [V]
pure wind	0m/s, 5m/s,10m/s	0
pure actuation	0m/s	-500,0,400,800
wind+actuation	10m/s	-500,0,400,800

4.3 Results

In this section, the measured wing deformations are plotted using wing fixed coordinate defined in Fig. 15. For the 'pure wind' condition, deformed shapes of the tail wing are shown in Fig. 16. As the wind speed got faster, the tail wing was bent to the –z direction. At the 5m/s, the magnitude of the tip bending was about 6.4mm(=0.46mm-(- 5.93mm)) compared to the 0m/s case, while the end deflection was 18.8mm at 10m/s. For the 'pure actuation' condition, tail wing was bent to the –z direction as the input voltage increased, because MFC actuator bent toward the –z direction at the plus voltage. Otherwise, when -500V was engaged, MFC actuator bent to the opposite side about 0.6mm. So, tail wing was bent to the +z direction as depicted in Fig. 17. From the results, it was found that approximately 5mm deflection could be induced by using MFC actuator. From the both 'pure wind' and 'pure actuation' condition, it was shown that the magnitudes of the bending induced by MFC actuator were smaller than that induced by wind. For 'wind+actuation' condtion at the wind speed of 10m/s, tail wing deformations were observed as varying input voltages. The tail wing was bent to the –z direction when the input voltages were 400V and 800V. Otherwise, tail wing was bent to the +z direction at the -500V as similar as 'pure actuation' condition (Fig. 18). The magnitudes of the bending from the 0V case were approximately 2.4mm at 800V, 1.5mm at 400V and -0.5mm at -500V, respectively.

From a series of experiments, it was observed that the 'flexible' tail wing was deformed according to the wind speeds and that attached MFC actuator could deform the tail wing. Consequently, MFC actuator could be used for controlling the tail wing shapes.

5. CONCLUSION

In this study, we developed a real-time point tracker system using commercial cameras. Four commercial IR CCD cameras were prepared with IR LEDs to track the markers in IR band for avoiding interferences by visible light. The measurement software was also prepared based on the specific point extraction and points matching algorithm with 3-D coordinates calculation method. From a series of verification tests, the performances of the developed system were evaluated that the point tracking uncertainty has been shown to be ±0.5mm. Consequently, we applied the real-time point tracker system to quantify the deformed shapes of the tail wing at which MFC actuator was attached. From the wind tunnel test with various wind speed and input voltage, it was found that MFC actuator could deform the tail wing curvature about 5mm at 0m/s and 3mm at 10m/s. The present real-time point tracker system provides a very economical but powerful solution to measure continuous deformation shapes of many engineering structures.

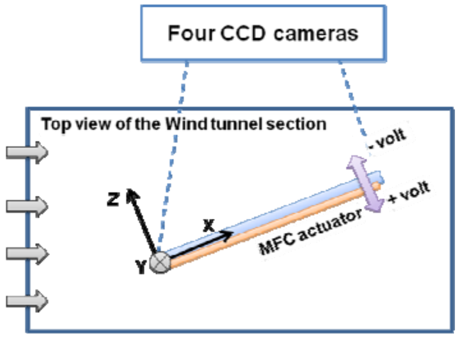

Fig. 15 (Top view) Installation of the tail wing on wind tunnel section and definition of the wing fixed coordinate

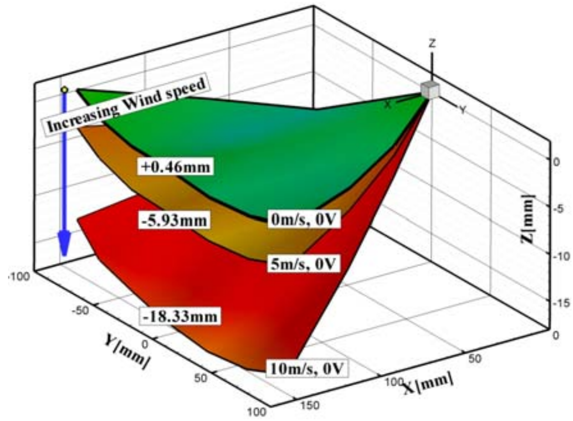

Fig. 16 Deformed shapes for 'pure wind' condition; the wind speeds are 0m/s, 5m/s, 10m/s at 0V.

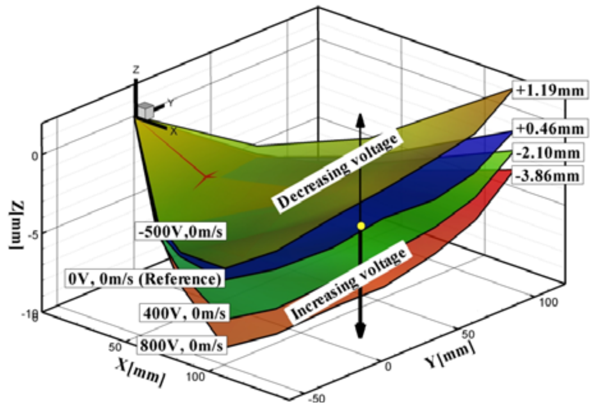

Fig. 17 Deformed shapes for 'pure actuation' condition; the input voltages of the MFC actuator are-500V, 0V, 400V and 800V at 0m/s.

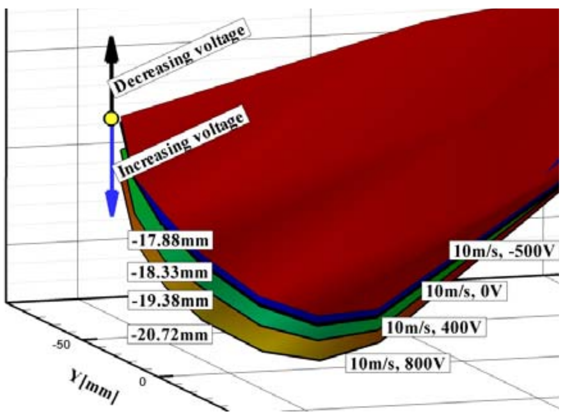

Fig. 18 Deformed shapes with MFC actuation of -500V, 0V, 400V, 800V at wind speed of 10m/s

ACKNOWLEDGMENTS

This study has been supported by KARI under the KHP Dual-Use Component Development Program funded by the Ministry of Knowledge Economy.

REFERENCES

[1] R. K. van der Draai, R. P. M. van Schinkel and A. Telesca, "A new approach to measuring model deflection," *18th International Congress on Instrumentation in Aerospace Simulation Facilities*, pp. 33/1~pp. 33/7, 1999

[2] G. A. Fleming and S. A. Gorton, "Measurement of Rotorcraft Blade Deformation using Projection Moiré Interferometry," *Proceedings of SPIE*, vol.3411, pp. 514-527, 1998

[3] G. A. Fleming, S. M. Bartman, M. R. Waszak and L. N. Jenkins, "Projection moiré interferometry measurements of micro air vehicle wings," *Proceedings of SPIE,* Vol. 4448-16, pp. 90-101, 2001

[4] O. Schneider, "Analysis of SPR measurements form HART II" *Aerospace Science and Technology*, Vol. 9, pp. 409-420, 2005.

[5] Camera Calibration Toolbox for MATLAB, http://www.vision.caltech.edu/bouguetj/calib_doc/

[6] R. Hartly and A. Zesserman, *Multiple View Geometry in Computer Vision*, Cambridge Press, 2003